Dry amyloid fibril assembly in a yeast prion peptide is mediated by long-lived structures containing water wires

Govardhan Reddy[a], John E. Straub[b], and D. Thirumalai[a,c,1]

[a]Biophysics Program, Institute for Physical Science and Technology, and [c]Department of Chemistry and Biochemistry, University of Maryland, College Park, MD 20742; and [b]Department of Chemistry, Boston University, Boston, MA 02215

Edited* by Harold A. Scheraga, Cornell University, Ithaca, NY, and approved October 22, 2010 (received for review June 18, 2010)

Amyloid-like fibrils from a number of small peptides that are unrelated by sequence adopt a cross-β-spine in which the two sheets fully interdigitate to create a dry interface. Formation of such a dry interface is usually associated with self-assembly of extended hydrophobic surfaces. Here we investigate how a dry interface is created in the process of protofilament formation in vastly different sequences using two amyloidogenic peptides, one a polar sequence from the N terminus of the yeast prion Sup35 and the other a predominantly hydrophobic sequence from the C terminus of Aβ-peptide. Using molecular dynamics simulations with three force fields we show that spontaneous formation of two ordered one-dimensional water wires in the pore between the two sheets of the Sup35 protofilaments results in long-lived structures, which are stabilized by a network of hydrogen bonds between the water molecules in the wires and the polar side chains in the β-sheet. Upon decreasing the stability of the metastable structures, water molecules are expelled resulting in a helically twisted protofilament in which side chains from a pair of β-strands in each sheet pack perfectly resulting in a dry interface. Although drying in hydrophobically dominated interfaces is abrupt, resembling a liquid to vapor transition, we find that discrete transitions between the liquid to one-dimensional ordered water in the nanopore enclosed by the two β-sheets to dry interface formation characterizes protofilament assembly in the yeast prions. Indeed, as the two sheets of the hydrophobic Aβ-sequence approach each other, fibril formation and expulsion of water molecules occur rapidly and nearly simultaneously.

amyloid fibrils | dewetting transition | electrostatic interactions | prion diseases

Many proteins and peptides that are unrelated by sequence or structure undergo remarkable conformational changes from their monomeric states to form a universal cross-β-structure, which is a characteristic of amyloid fibrils (1–3). Unlike the folding of monomeric peptides in which self-assembly is predominantly driven by the need to sequester the hydrophobic residues from water (4, 5), the interactions and the cascade of events that lead to fibril formation are considerably more complex (6). Both hydrophobic and electrostatic interactions, especially through formation of a network of hydrogen bonds (7, 8), stabilize the amyloid fibrils. The common global architecture of fibrils and the demonstration that almost any protein can form fibrils under suitable external conditions are sometimes taken as evidence that backbone hydrogen bonding must drive both the thermodynamics and kinetics of their formation. However, it is now realized that a subtle interplay between nonspecific hydrophobic forces, the stereospecific sequence-dependent hydrogen bond, and water-mediated interactions are important in determining the mechanisms and kinetics of assembly into ordered aggregated structures (8–10). Although there are significant sequence-dependent variations in the rates of fibril formation (2, 11), high-resolution structures of microcrystals grown from peptide fragments from a variety of proteins show that they share a common structure of the cross-β-spine with a remarkably dry interface between the two sheets (8). How does water mediate the formation of nearly identical cross-β-amyloid structures from vastly different sequences? In order to answer this question, we study the association kinetics of preformed β-sheets of two peptides, one of which is polar and the other is predominantly hydrophobic.

Water plays a variety of roles in the folding of proteins (4) and the assembly of multidomain proteins (12, 13). During protein folding, a few water molecules are sometimes trapped in the interior of proteins upon collapse of the polypeptide chains giving rise to a "wet" globule. The squeezing out of the water molecules then becomes rate-determining in the final stages of folding (14). In the assembly of multidomain proteins, several possibilities arise depending upon the nature of the interface and the surface topography (13). The length scale variations in hydrophobic interactions that mediate the formation of multidomain proteins have been illustrated using the two domain enzyme BphC (15) and the collapse of a melittin tetramer (16). During the interdomain formation process in BphC enzyme, with preformed monomers, the number of trapped water molecules decreases continuously as the domains approach each other (15). In contrast, there is an abrupt dewetting transition as the melittin domains approach each other to form a compact tetramer, which is in accord with theoretical predictions for association of large (>1 nm) structureless hydrophobic objects in water (12, 17–19).

In interfaces between β-sheets in amyloid-like oligomers (for example, the central hydrophobic cluster ^{16}KLVFFAE^{22} from the Aβ-peptide; refs. 20–22) and fibrils formed by predominantly hydrophobic sequences ($A\beta_{37-42}$, for example, ref. 8), a drying-like transition occurs. Although these findings support the notion that extended hydrophobic surfaces are required for dewetting transition (12), the discovery of a totally dry environment between the β-sheets of amyloid fibrils formed by the polar heptapeptide, GNNQQNY [residues (7–13) from the prion domain of Sup35), is a surprise (7, 8). In order to illustrate how water mediates protofilament formation in amyloidogenic peptides, we study the association kinetics of preformed β-sheets of GNNQQNY and GGVVIA [residues (37–42) from the C terminus of the Aβ peptide], which are structureless as monomers. The structure of the GNNQQNY cross-β-spine (prion fibril or PF) shows a remarkable interlocking of the two β-strands to form a steric zipper in which the side chains from the two sheets fully interdigitate with one another, thus giving rise to a dry interface (7). Despite the drastically different chemical character of the

Author contributions: D.T. designed research; G.R. and D.T. performed research; G.R., J.E.S., and D.T. contributed new reagents/analytic tools; G.R., J.E.S., and D.T. analyzed data; and G.R., J.E.S., and D.T. wrote the paper.

The authors declare no conflict of interest.

*This Direct Submission article had a prearranged editor.

[1]To whom correspondence should be addressed. E-mail: thirum@umd.edu.

This article contains supporting information online at www.pnas.org/lookup/suppl/doi:10.1073/pnas.1008616107/-/DCSupplemental.

two sequences, their architectures in the fibril state are virtually identical. Assembly of preformed sheets of the polar sequence occurs by multiple routes and involves formation of metastable structures that are stabilized by favorable interactions between two one-dimensional water wires and inward-pointing polar side chains. In sharp contrast, protofilament formation and expulsion of water molecules resulting in a dry interface in the predominantly hydrophobic Aβ-sequence, which forms an $A\beta_{37-42}$ fibril (AF) occurs rapidly and nearly simultaneously.

Results and Discussion

Assembly Kinetics of Prion Fibril Is Heterogeneous. The sheets in the protofilaments of the PF, which are initially arranged in a planar conformation (7, 8) with $\delta D(0) = D_S(0) - D_E = 0.8$ Å ($D_E =$ 10.0 Å is the distance between the centers of mass in the crystal structures of the two sheets, and $D_S(0)$ is the corresponding distance at the start ($t = 0$) of the simulation) acquired a spontaneous helical twist (23) at $t \approx 1.5$ ns as $\delta D(t)$ decreases to zero (Figs. 1 and 2). The global conformation of the protofilament is specified using ($\delta D(t)$, Φ, Ψ), where the helical angle Φ is the relative orientation of the helical axes of the two sheets, and Ψ is the intrinsic twist angle in a β-sheet (Figs. 1 and 2). The angle $\Phi = \cos^{-1}[\hat{r}_{36}^{Q4(C\alpha)}(1) \cdot \hat{r}_{36}^{Q4(C\alpha)}(2)]$, where $\hat{r}_{36}^{Q4(C\alpha)}(1)$ and $\hat{r}_{36}^{Q4(C\alpha)}(2)$ are the unit vectors in β-sheets 1 and 2, respectively, join the C_α atom of residue Q4 in peptides 3 and 6 in each sheet (Fig. 1). The twist angle $\Psi = \cos^{-1}(\sum_{j=1}^{2}\sum_{i=3}^{5}[\hat{r}_{Y7_{C\alpha}N2_{C\alpha}}^{(i)}(j) \cdot \hat{r}_{Y7_{C\alpha}N2_{C\alpha}}^{(i+1)}(j)]/6)$, with $\hat{r}_{Y7_{C\alpha}N2_{C\alpha}}^{(i)}(j)$ being the unit vector joining the C_α atoms of the residues N2 and Y7 in peptide i in sheet j. When the two sheets are fully associated $\delta D(t \to \infty) = 0$ the equilibrium values of Φ_o and Ψ_o are 14.5° (black curve in Fig. 1*B*) and 10.53° (black curve in Fig. 1*C*), although there are small (≈1°) variations depending on the force field (Fig. 2 and Table S1).

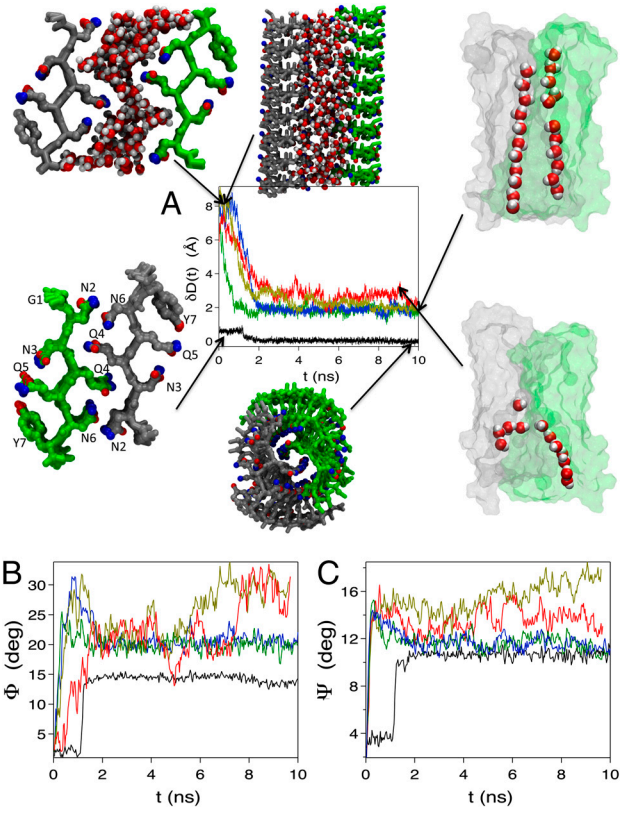

Fig. 1. (*A*) Time evolution of the center of mass distance between the two β-sheets for a few trajectories with varying $\delta D(0)$. The black curve is for $\delta D(0) = 0.8$ Å, the distance in the crystal structure. The values of $\delta D(0)$ are 6.2 Å for the trajectories in red and green and 8.0 Å for the ones in blue and gold. Ordered water wires form in the trajectories in green and blue. Top views of the solvated and dry steric zipper are shown on the upper and lower left, respectively, and a side view of the initial structure with $\delta D(0) = 8.0$ Å is in the center. The metastable structure on the top shows trapped water wires, whereas the lower right shows water in a disordered arrangement in the pore. The equilibrium structure of the protofilament with a helical twist ($\delta D(t \to \infty) = 0$) is in the lower center. (*B*) Time-dependent changes in the helical angle, $\Phi(t)$ as the two sheets associate. (*C*) Time evolution of the twist angle, $\Psi(t)$, during the protofilament formation. Colors for the trajectories used are described in *A*.

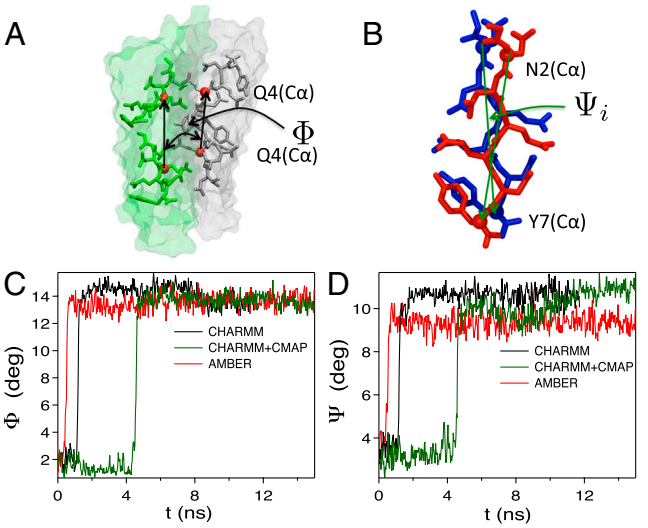

Fig. 2. Helical and twist angles for various force fields. (*A*) The two β-sheets are shown in green and silver color. Peptides 3 and 6 in each sheet are in licorice representation. The C_α atom of residue Q4 in red is shown in van der Waal representation. The two arrows represent the vector joining the C_α atoms of residue Q4 in peptides 3 and 6 in each sheet. The angle between the two vectors represented by the arrows is Φ, the helical angle. (*B*) The peptides shown in red and blue are the two adjacent peptides in a β-sheet. In each peptide, the C_α atoms of residues N2 and Y7 are shown in van der Waal representation. Each arrow represents the vector joining the C_α atoms of residues N2 and Y7 in each peptide. Ψ_i is the angle between the two vectors. To obtain the twist angle Ψ, we average Ψ_i of all the adjacent strands in the both the β-sheets. (*C*) Angle between the two β-sheets, Φ, and (*D*) twist angle in a sheet, Ψ, as a function of time for different force fields for $\delta D(0) = 0.8$ Å. The protofilaments acquire a spontaneous twist (see Fig. 1*A*) in all force fields. There are small variations in the equilibrium values of Φ_o and Ψ_o.

Association kinetics of the two sheets, described by the time-dependent decrease of $\delta D(t)$ shows considerable heterogeneity in the assembly pathways depending on $\delta D(0)$, which in the simulations range from 3.8 to 8.0 Å. The heterogeneity results in distinct ways in which the two β-sheets pack. When $\delta D(0) \lessapprox 5$ Å, we observe that the association between the two sheets occurs in a parallel manner, i.e., Φ and Ψ fluctuate around 19.5° (Fig. 1*B*) and 12.1° (Fig. 1*C*), respectively, at long times. In this pathway, after a rapid initial decrease in the intersheet distance, $\delta D(t)$ saturates to 2–3 Å and the resulting metastable structure is characterized by the formation of two water wires in the channel between the β-sheets. For larger $\delta D(0)$, the probability of protofilament assembly with $\Phi > 19.5°$ increases substantially, which in turn leads to defects in the packing of the two sheets. In structures with trapped water molecules containing packing defects, Φ and Ψ fluctuate around 30.2° and 16.0°, respectively (Fig. 1 *B* and *C*), which are substantially greater than the equilibrium Φ_o and Ψ_o values. The percentage of trajectories in which water wires are formed depends on $\delta D(0)$. In all the trajectories ordered water wires form when $\delta D(0) = 3.8$ Å, whereas when $\delta D(0)$ increases to 6.2 Å (8.0 Å) in only 43% (9%) of the structures have long-lived water wires. Note that $\delta D(0) = 8.0$ Å corresponds to initial sheet separation of 18.0 Å. At these distances, the interaction energy between the sheets is negligible. Thus, our simula-

tions probe unbiased formation of protofilaments dictated solely by classical dynamics and a chosen force field.

Metastable Structures Are Stabilized by Water Wires. When the sheets approach each other in a parallel manner, complete association with $\delta D(t \to \infty) = 0$ leading to a dry interface is not observed even for $t \approx 100$ ns in most of the trajectories. The failure of $\delta D(t)$ to reach zero even after $t \approx 100$ ns is surprising especially given that complete dewetting in melittin tetramers (16) whose initial separation $\delta D(0)$ is in the range of 4–6 Å, occurs in ≈0.3–0.4 ns. Examination of the simulation snapshots (Fig. 3*A*) shows that the remarkably different behavior in the assembly of the β-sheets, characterized by a dry polar interface in the equilibrium structure of the PF, is due to trapping of water in the nanopore between the two β-sheets of the protofilament. The trapped water molecules form two well-ordered one-dimensional wires (Fig. 3*A*). The structural characteristics of the water wires, which form in the groove made up of the backbone atoms of N2, N3, and Q4, and the side chains of N2 and Q4 associated with the β-sheets (Fig. 3*A*), exhibit several features of one-dimensional order. First, the water density in the trapped water wire along the z axis, which is aligned along the protofilament axis, is stunningly periodic with a spacing (≈3 Å) corresponding approximately to the size of the water molecule (Fig. 3*B*). Assuming that the pore is roughly cylindrical, with a constant radius R (Fig. 3*C*), we calculated $\rho(z) = N(z)/\pi R^2 \Delta z$, where Δz is a length element along the z axis and $N(z)$ is the number of water molecules in the volume $\pi R^2 \Delta z$. The density profile does not change as long as a reasonable value of R is chosen. Second, a water molecule in a given wire forms two hydrogen bonds with the neighboring molecules. In addition, water molecules in the pore also form two other hydrogen bonds, one with the carbonyl oxygen of the N3 backbone, which is part of the groove and the other with the O and NH in the amide group of the Q4 of the adjacent β-strand (Fig. 3*A*). Third, the macrodipoles of the two wires are aligned in the direction opposite to the protofilament axis. The distribution $P[\cos(\theta)]$, with θ being the angle between the macrodipoles of the water wires, shows that they are predominantly parallel to each other (Fig. 3*D*). Taken together, the picture that emerges is that the saturation of $\delta D(t)$ at long times is associated with the spontaneous formation of stable ordered water wires in the channel of the protofilament. Such a structure must be metastable because the ground state corresponds to a twisted double β-sheet with a dry interface, i.e., $\delta D(t \to \infty) = 0$ (structure in the lower center in Fig. 1*A*). The qualitative nature of the results do not depend on the force field or the ensemble in which the simulations are carried out (see Figs. S1 and S2).

The structural integrity of the water wires is also reflected in the stabilities of the water molecules that are spontaneously trapped in the nanochannel for long times. Comparison of the distributions of the binding energy, E_B, which is the interaction potential per water molecule in the bulk and the pore shows that it is favorable to localize the water in the polar channel (Fig. 3*E*). The average binding energy of the water in the wires is less than in

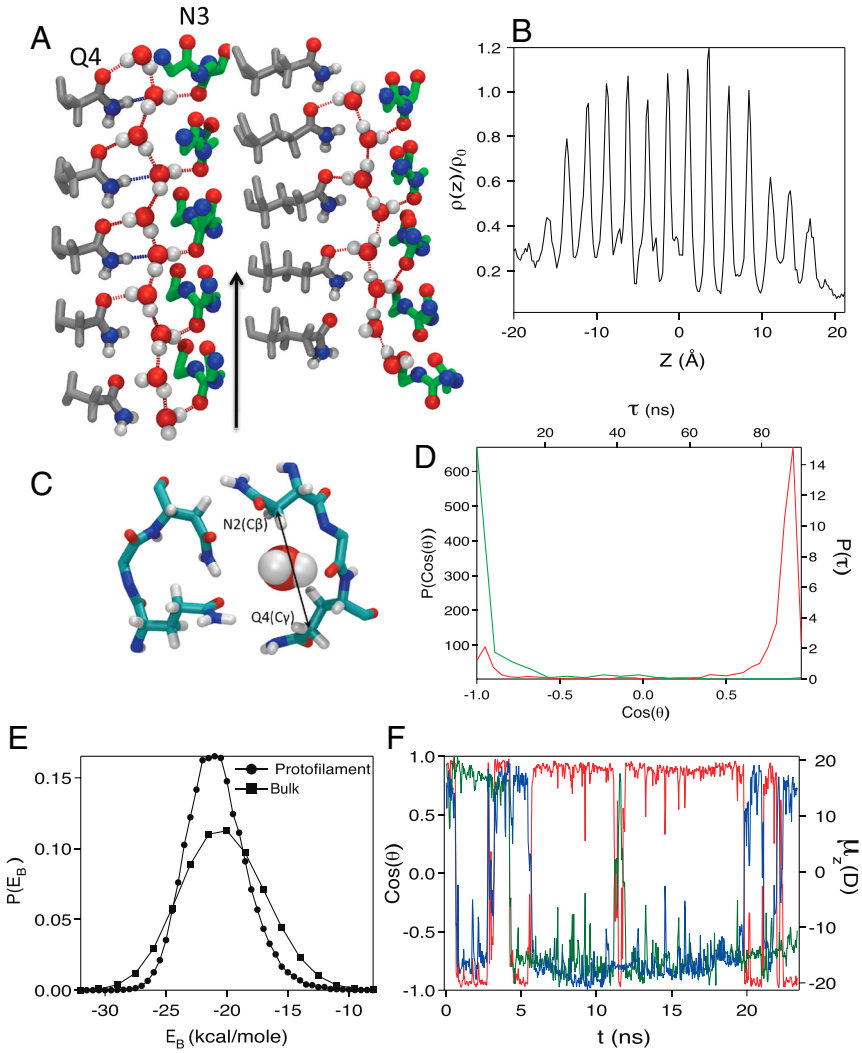

Fig. 3. Water wire properties. (*A*) Hydrogen bonding pattern in the water wire in two orientations. Water molecules in the wire form hydrogen bonds with the backbone carbonyl oxygen of N3, and with the carbonyl oxygen and –NH hydrogen in the amide group of the side chain of Q4 from the opposing β-strand. The arrow shows the direction of the protofilament axis. (*B*) Density of water in one of the water wires along the protofilament axis. The bulk water number density, ρ_0, is 0.0334 Å^{-3}. (*C*) The pore diameter used to calculate the normalization constant is 5.5 Å which is the difference in the distance between the C_β atom of residue N2 and C_γ atom of residue Q4 ($d_{C\beta-C\gamma} = 7.672$ Å) and the van der Waal radius of carbon atom ($d_C = 2.175$ Å). (*D*) Probability distribution of the cosine of the angle between the two water wire macrodipoles in red shows that the water wires are predominantly parallel. Lifetime distribution ($P(\tau)$) of the water molecules in the wire is shown in green (time axis is at the top and $P(\tau)$ is on the right side of the figure). (*E*) Distribution of the binding energy of the water molecules, $P(E_B)$, involved in the formation of the water wire and the bulk water. The average binding energy, $\langle E_B \rangle$, of the water molecule in bulk and in the protofilament is −19.53 and −20.56 kcal/mole, respectively. (*F*) Change in the cosine of the angle between the two water wire macrodipoles, $\cos(\theta)$, as a function of time is shown in red. Time evolution of the z component of the dipole moment of the two water wires in debye units is shown in blue and green.

the bulk by about 1 kcal/mole, thus making entry into the pore favorable despite a loss in entropy due to localization in the pore. The gain in average binding energy upon the water wire formation in the polar channel is in sharp contrast to the water chain formation in an open carbon nanotube (CNT) (24) which shows a loss in average binding energy. However, filing of water depends on free energy of transfer from the bulk to the pore, which is determined by the distribution of binding energies of water in the channel (or CNT) and in the bulk phase. Spontaneous formation of water wire in the polar channel studied here is energetically favorable as it is for the water wire in a narrow open CNT (25). Indeed, a sharp increase in the free-energy cost to remove a water molecule from the wires readily explain the extraordinarily long lifetimes of the metastable structures.

Spontaneous Coherent Flipping Dynamics of Water Wires. Water molecules in the wires continuously undergo exchange with the bulk water by a relay mechanism, i.e., in which the water molecules at the edge of the channel are replaced by bulk water. The lifetimes (time a given water molecule is in the nanochannel $-20 < z < 20$ Å) is broadly distributed with an average $\langle\tau\rangle \approx 7.0$ ns (Fig. 3*D*). The residence times of the water at the ends of the pore are short, whereas those in the interior exceed 10 ns. The number of water molecules in each wire is $N_w \approx 10$. If the wire is perfectly one-dimensional, we expect that the macrodipole $\mu_w \approx 10\mu_o$, where μ_o is the dipole moment of the isolated water, which in the TIP3P is 2.35 D. Using simulations, we determined that $\langle\theta_{i,i+1}\rangle$, the average angle between successive water molecules in the wire, is ≈68° (Fig. S3). Thus, the dipole moment of a water molecule projected along the protofilament axis is $\mu^z \approx \mu_o \cos\langle\theta_{i,i+1}/2\rangle \approx 1.94$ D, which implies that the expected value of the macrodipole of the wire, $\mu_w^z = 10\mu^z \approx 19.4$ D. This value is in accord with the simulations, which again confirms that the waters in the wire are arranged in an one-dimensional array (Fig. 3*F*). Interestingly, μ_w^z for each wire, which is predominantly aligned in a direction antiparallel to the fibril axis, flips spontaneously. In the process, the magnitude of μ_w^z is unchanged, which shows that the flipping dynamics is coherent on the length scale of the pore. Fig. 3*F* shows that $\cos\theta(t)$ fluctuates between +1 and −1 with the parallel arrangement ($\cos\theta(t) \approx +1$) being the dominant conformation. Even though flipping dynamics involves 10 water molecules, the average duration of flip is only ≈5–10 ns. Thus, the water wires undergo large mesoscale rearrangements on very short time scales without significantly affecting the one-dimensional order.

Electrostatic Interactions Stabilize the Metastable Prion Fibrils. In order to illustrate how water molecules in the wires file out to create the dry interface and in the process demonstrate that the electrostatic interactions render the polar Sup35 protofilaments stable, we systematically varied the strength of the water peptide electrostatic interactions (26) (see *Methods* for details), measured as a fraction (λ_E) of the full ($\lambda_E = 1$) value (Fig. 4). When $0 \le \lambda_E \le 0.25$, the water molecules file out of the nanopore in a continuous manner in $t \approx 0.5$–2 ns. If fluctuations in the solvent-exposed edge β-strands block the nanopore, then expulsion of water occurs in discrete steps (see Movie S1 illustrating the orderly exit of water molecules), a finding that dominates as λ_E increases (Fig. 4). There is considerable heterogeneity both in the duration of the steps and in the number of water molecules that file out in each step. For $\lambda_E = 0.75$, the time needed to empty the nanopore lengthens. In some trajectories, a stable water wire persists for $t \approx 20$ ns. These results show that the water wires ($\lambda_E = 1$) are stabilized by favorable electrostatic interactions with the residues in the β-sheets. Upon formation of the protofilament, with a perfectly dry interface, the water peptide hydrogen bonds are replaced by favorable interpeptide interactions.

The association between the two β-sheets in a large fraction of the trajectories leads to defective packing [$\Psi(t) > 19.5°$ and $\Psi > 12.1°$] if $\delta D(0) \gtrapprox 5$ Å (data in red and gold in Fig. 1 *B* and *C*). Although $\delta D(t)$ decreases rapidly in these trajectories (Fig. 1*A*), perfect water wires are not observed in the protofilament pores. However, several water molecules are trapped between the sheets in a disordered state (see Fig. 1*A*). The most likely mechanism for escape of the trapped water molecules is through the gap between the misaligned β-sheets (see Fig. S4 and Movie S2 of a sample trajectory). Taken together, the simulations show that water plays distinct roles in the heterogeneous assembly of the polar protofilament. When water is trapped in the ordered state, it inhibits the formation of the dry interface where as it serves as a lubricant facilitating the formation of a dry steric zipper if the two sheets are initially misaligned to some extent.

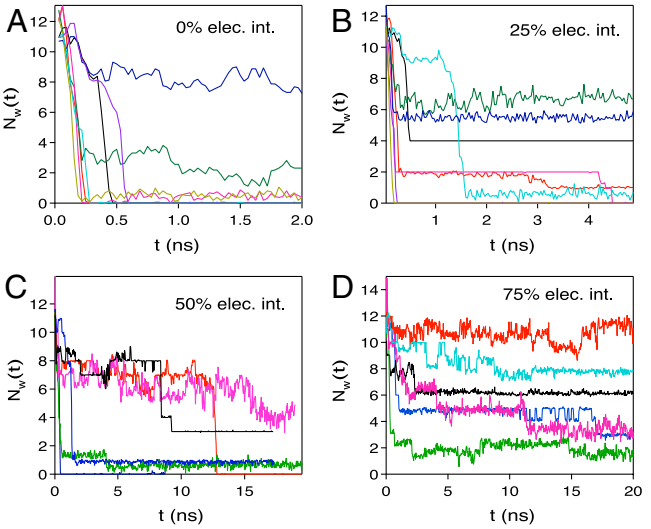

Fig. 4. Number of water molecules in the wire as a function of time at different strengths (λ_E) of the electrostatic interaction between the Sup35 monomers in the protofilament and water. *A–D* are for 0%, 25%, 50%, and 75% of the full ($\lambda_E = 100\%$ of the electrostatic interaction strength.

Expulsion of Water Molecules and Fibril Formation in Aβ-Peptide Coincide. In order to contrast the assembly mechanism of the polar PF with the formation of AF, we simulated the kinetics of association of β-sheets from the sequence GGVVIA in the carboxy terminus of $A\beta_{37-42}$. The steric zipper (referred to as "face to back" packing in ref. 8) involves interdigitation of residues V4 from one strand (green in Fig. 5) with the hydrophobic residues V3 and I5 (gray in Fig. 5). In contrast to the assembly of PF, the two sheets in the AF, with $\delta D(0) = 3.88$ and 6.24 Å, associate with one another in less than 3 ns (Fig. 5). The fluctuations in G1 and G2 lead to instability in the edges of the β-sheets, which results in dispersion in $\delta D(t)$ even after association and drying transitions are complete. Protofilament formation involving the two sheets is driven by hydrophobic forces, which leads to packing of V4 from one sheet against V3 and I5 from the adjacent β-sheet. Fig. 5 shows that, for both the values of $\delta D(0)$, the time at which the number of water molecules around the bulky hydrophobic residues vanishes coincides with complete association of the two sheets ($\delta D(t) \approx 0$). Thus, unlike in the PF formation, the assembly of the two sheets and expulsion of water molecules occur nearly simultaneously. The kinetics of association of β-sheets in AF is reminiscent of oligomer formation in $A\beta_{16-22}$ peptides (20) in which the time scale for coil → strand formation and decrease in the number of water molecules between two β-strands coincide. In both oligomer and AF formation, water expulsion occurs rapidly and is driven by the favorable interaction between the bulky hydrophobic residues. The mechanism of rapid expulsion of water molecules in the AF is due to the nonspecific hydrophobic interaction, whereas in PF metastable formation of water

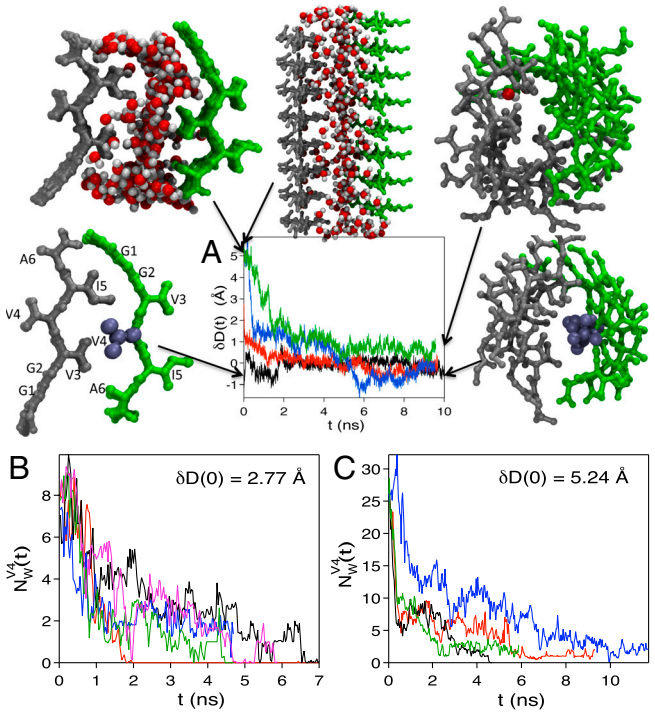

Fig. 5. Association kinetics of the amyloid fibril. (*A*) Time evolution of the center of mass distance between the two β-sheets in the Aβ_{37-42} protofilament with $D_E = 9.34$ Å. The trajectory with $\delta D(0) = 0$ Å as in the crystal structure is in black. Data in blue and green are for $\delta D(0) = 5.24$ Å and the trajectory in red corresponds to $\delta D(0) = 2.77$ Å. The solvated initial conformations with the top and side views are on the upper left and in the center, respectively. The top view of the protofilament at equilibrium is displayed on the lower left. The equilibrium protofilament structure, with a small helical twist, is on the bottom right, whereas the endpoint structure for the green trajectory shows the presence of trapped water molecules. Residue V4 in one of the β-strands shown in van der Waal representation is in the interior of the protofilament to emphasize packing of hydrophobic residues. (*B*) Number of water molecules within 3.5 Å of residue V4 for $\delta D(0) = 2.77$ Å. (*C*) Number of water molecules within 3.5 Å of residue V4 for $\delta D(0) = 5.24$ Å. The interior of the protofilament becomes dry as the two β-strands associate. The colors in *B* and *C* correspond to the trajectories in *A*.

wires stabilized by a favorable stereospecific network of hydrogen bonds involving water molecules and polar side chains results in slow association.

Concluding Remarks

Our work has several implications. First, based on the dewetting time scales found in this work, we surmise that AF can form nearly a 1,000 times faster than the PF. The spontaneously formed metastable intermediate structures, with ordered trapped water wires throughout the nanopore, create a barrier to rapid assembly in the PF that is absent in the AF. Second, the heterogeneous assembly of the two β-sheets also suggests plausible routes to polymorphism and prion strains. In the case of PF, the alternate packing of the two sheets with large twist and helical angles might represent an example of prion strains. It is likely that a discrete number of trapped water molecules might also be a part of the alternate polymorphic structures as has been observed in a recent 2D infrared study of Aβ_{1-42} structures (27). Third, the heterogeneous assembly for protofilament formation discussed here might reflect one of the routes by which PF and AF form. Indeed, such events have been observed in simulations of amyloid fibril formation in coarse-grained models (28), which have provided considerable insight into protein aggregation (29). Finally, it is interesting to note that there is a striking resemblance between the structure of the water wires in the PF and the single water wire found in human aquaporin, hAQP4 (see Fig. S5). The water wire in the center of one side of the channel in hAQP4 is stabilized by hydrogen bond network (30) that is similar to that found in PF. However, the hydrophobic residues that line the opposite side of the channel in hAQP4 render the wire unstable compared to the ones found in PF. The decreased stability is needed to achieve flow of water through the aquaporin channel.

Methods

Simulation Details. We performed all atom molecular dynamics (MD) simulations of protofilament formation in Sup35 and Aβ_{37-42} monomers to reveal the molecular events that occur as the two sheets approach each other. The protofilaments are constructed from two β-sheets, with each containing eight β-strands, using the microcrystal structures of PF and AF as starting structures. The separation, D_E, between the centers of mass in the initial structures of the two sheets is increased to D_S. The energy of the system is minimized and water molecules are equilibrated for 1 ns with $\delta D(0) = D_S(0) - D_E$ fixed. We emphasize (see *SI Text* for details) that the restraints are used only during the equilibrium phase. The restraints that keep $\delta D(0)$ fixed during the equilibration process are released and the energy of the whole system is minimized using the conjugate gradient method. Subsequently, the entire system of water and peptides are allowed to move as demanded by the classical equations of motion. Thus, the structures that are sampled during the simulations are determined solely by the force field.

The time-dependent decrease in $\delta D(t)$ is used to study the details of the association kinetics. In silico alterations of interactions between the peptides and water, which are impossible to achieve in experiments, are used to provide insights into the nature of interactions that stabilize amyloid fibrils and the intermediate structures with different sequences and identical final structures. Results are presented using the CHARMM PARAM 22 force field generated in the NVT ensemble. To establish that the conclusions are robust, the simulations were also performed using three force fields in both NVT and NPT ensembles (*SI Text* contains the relevant results).

Role of Electrostatic Interaction. We performed simulations in which the electrostatic interactions between the water and the peptides are varied using the Free Energy Perturbation module in NAMD2.7b1. These simulations were done only for the PF. The Hamiltonian for the protofilament in water (say state T) is $H_T = H_w + H_p + H_{wp}^{vdw} + H_{wp}^{E}$. Here H_w is the interaction between the water molecules, H_p is the interaction between the atoms in the protofilement, H_{wp}^{vdw} is the van der Waals interaction between the atoms in water molecules and in the protofilament, and H_{wp}^{E} is the electrostatic interaction between the atoms in water molecules and in the protofilament.

We define λ_E through the relation $H_{\lambda_E} = H_T + (\lambda_E - 1)H_{wp}^{E}$. The absence of H_{wp}^{E} implies $\lambda_E = 0$, whereas $\lambda_E = 1$ is equivalent to retaining the full strength of the electrostatic interactions. Thus, by tuning λ_E, the effect of electrostatic interactions on the stability of the water wires can be examined. When $\lambda_E = 0$, 0.25, 0.5, and 0.75, the strength of the electrostatic interaction between the water and protofilament is 0%, 25%, 50%, and 75% of the actual electrostatic interaction strength. Simulations at the desired electrostatic interaction strength between the protofilament and water are performed by integrating the equations of motion using H_{λ_E}.

ACKNOWLEDGMENTS. We thank Dr. Michael Hinczewski, Dr. Riina Tehver, and Prof. John D. Weeks for useful discussions. This work was supported by a grant from the National Institutes of Health (R01GM076688-05) and the National Science Foundation (CHE 09-14033). A portion of this research was conducted at the Center for Nanophase Materials Sciences, which is sponsored at Oak Ridge National Laboratory by the Division of Scientific User Facilities, US Department of Energy through Grant CNMS2007-048. Part of the computational work was done by using the resources of National Science Foundation Teragrid through Grant TG-MCB080035N.

1. Tycko R (2006) Molecular structure of amyloid fibrils: Insights from solid-state NMR. *Q Rev Biophys* 39:1–55.
2. Chiti F, Dobson CM (2009) Amyloid formation by globular proteins under native conditions. *Nat Chem Biol* 5:15–22.
3. Bennett MJ, Sawaya MR, Eisenberg D (2006) Deposition diseases and 3D domain swapping. *Structure* 14:811–824.
4. Dill KA (1990) Dominant forces in protein folding. *Biochemistry* 29:7133–7155.
5. Dill KA, Ozkan SB, Shell MS, Weikl TR (2008) The protein folding problem. *Annu Rev Biophys* 37:289–316.
6. Thirumalai D, Klimov DK, Dima RI (2003) Emerging ideas on the molecular basis of protein and peptide aggregation. *Curr Opin Struct Biol* 13:146–159.

7. Nelson R, et al. (2005) Structure of the cross-β spine of amyloid-like fibrils. *Nature* 435:773–778.
8. Sawaya MR, et al. (2007) Atomic structures of amyloid cross-β spines reveal varied steric zippers. *Nature* 447:453–457.
9. Balbirnie M, Grothe R, Eisenberg D (2001) An amyloid-forming peptide from the yeast prion sup35 reveals a dehydrated β-sheet structure for amyloid. *Proc Natl Acad Sci USA* 98:2375–2380.
10. Reddy G, Straub JE, Thirumalai D (2009) Dynamics of locking of peptides onto growing amyloid fibrils. *Proc Natl Acad Sci USA* 106:11948–11953.
11. Chiti F, Stefani M, Taddel N, Ramponi G, Dobson CM (2003) Rationalization of the effects of mutations on peptide and protein aggregation rates. *Nature* 424:805–808.
12. Berne BJ, Weeks JD, Zhou RH (2009) Hydrophobic interactions and dewetting between plates with hydrophobic and hydrophilic domains. *Annu Rev Phys Chem* 60:85–103.
13. Cheng YK, Rossky PJ (1998) Surface topography dependence of biomolecular hydrophobic hydration. *Nature* 392:696–699.
14. Levy Y, Onuchic JN (2006) Water mediation in protein folding and molecular recognition. *Annu Rev Biophys Biomol Struct* 35:389–415.
15. Zhou R, Huang X, Margulius CJ, Berne BJ (2004) Hydrophobic collapse in multidomain protein folding. *Science* 305:1605–1609.
16. Liu P, Huang X, Zhou R, Berne BJ (2005) Observation of a dewetting transition in the collapse of the melittin tetramer. *Nature* 437:159–162.
17. Wallqvist A, Berne BJ (1995) Computer simulation of hydrophobic hydration forces on stacked plates at short-range. *J Phys Chem* 99:2893–2899.
18. Lum K, Chandler D, Weeks J (1999) Hydrophobicity at small and large length scales. *J Phys Chem B* 103:4570–4577.
19. Chandler D (2005) Interfaces and the driving force of hydrophobic assembly. *Nature* 437:640–647.
20. Klimov DK, Thirumalai D (2003) Dissecting the assembly of $A\beta_{16-22}$ amyloid peptides into antiparallel β sheets. *Structure* 11:295–307.
21. Krone MG, et al. (2008) Role of water in mediating the assembly of Alzheimer amyloid-β $A\beta_{16-22}$ protofilaments. *J Am Chem Soc* 130:11066–11072.
22. Klimov DK, Straub JE, Thirumalai D (2004) Aqueous urea solution destabilizes $A\beta_{16-22}$ oligomers. *Proc Natl Acad Sci USA* 101:15335–15340.
23. Esposito L, Pedone C, Vitagliano L (2006) Molecular dynamics analyses of cross-β-spine steric zipper models β-sheet twisting and aggregation. *Proc Natl Acad Sci USA* 103:11533–11538.
24. Hummer G, Rasaiah JC, Noworyta JP (2001) Water conduction through the hydrophobic channel of a carbon nanotube. *Nature* 414:188–190.
25. Rasaiah JC, Garde S, Hummer G (2008) Water in nonpolar confinement: From nanotubes to proteins and beyond. *Annu Rev Phys Chem* 59:713–740.
26. Waghe A, Rasaiah JC, Hummer G (2002) Filling and emptying kinetics of carbon nanotubes in water. *J Chem Phys* 117:10789–10795.
27. Kim YS, Liu L, Axelsen PH, Hochstrasser RM (2009) 2D IR provides evidence for mobile water molecules in β-amyloid fibrils. *Proc Natl Acad Sci USA* 106:17751–17756.
28. Bellesia G, Shea JE (2009) Diversity of kinetic pathways in amyloid formation. *J Chem Phys* 131:111102-1–111102-4.
29. Dima RI, Thirumalai D (2002) Exploring protein aggregation and self-propagation using lattice models: Phase diagram and kinetics. *Prot Sci* 11:1036–1049.
30. Ho JD, et al. (2009) Crystal structure of human Aquaporin-4 at 1.8 Å and its mechanism of conductance. *Proc Natl Acad Sci USA* 106:7437–7442.